

## Characterization of Interfacial Structure in Polymer-Fullerene Bulk Heterojunctions via $^{13}\text{C}$ $\{^2\text{H}\}$ Rotational Echo Double Resonance NMR

R. C. Nieuwendaal,<sup>1,\*</sup> D. M. DeLongchamp,<sup>1</sup> L. J. Richter,<sup>1</sup> C. R. Snyder,<sup>1</sup> R. L. Jones,<sup>1</sup> S. Engmann,<sup>1</sup> A. Herzing,<sup>2</sup> M. Heeney,<sup>3</sup> Z. Fei,<sup>3</sup> A. B. Sieval,<sup>4</sup> and J. C. Hummelen<sup>5</sup>

<sup>1</sup>Materials Science and Engineering Division, National Institute of Standards and Technology, 100 Bureau Drive, Gaithersburg, Maryland 20899, USA

<sup>2</sup>Surface and Microanalysis Science Division, National Institute of Standards and Technology, 100 Bureau Drive, Gaithersburg, Maryland 20899, USA

<sup>3</sup>Department of Chemistry, Imperial College, London SW7 2AZ, United Kingdom

<sup>4</sup>Solenne BV, Zernikepark 6-8, 9747AN Groningen, Netherlands

<sup>5</sup>Stratingh Institute for Chemistry, University of Groningen, Nijenborgh 4, 9747 AG Groningen, Netherlands



(Received 9 January 2018; published 13 July 2018)

We introduce a new application of solid state NMR measurements towards characterizing the donor-acceptor interfaces within bulk heterojunction (BHJ) films. Rotational echo double resonance (REDOR) is used to measure dipolar couplings between  $^{13}\text{C}$  nuclei on the acceptor phenyl- $\text{C}_{60}$ -butyric acid methyl ester (PCBM) fullerene cage, which is  $\approx 18\%$  isotopically enriched with  $^{13}\text{C}$ , and beta hydrogens on the donor poly(3-hexyl thiophene) (P3HT) main chain, which are  $>95\%$  isotopically enriched with  $^2\text{H}$ . The  $^{13}\text{C} - ^2\text{H}$  dipolar couplings are used for constraining possible models of molecular packing in the amorphous mixed phase of a P3HT/PCBM BHJ. The films studied are highly mixed ( $>80\%$ ) and have a maximum length scale of composition nonuniformity of  $\approx 6$  nm in the mixed phase, as demonstrated by  $^1\text{H}$  spin diffusion NMR and supported by TEM. The REDOR results show that despite the lack of phase separation at length scales greater than  $\approx 6$  nm, neat P3HT and PCBM clusters exist on  $\approx 3$  nm size scales, and, for the average PCBM molecule, the number of nearest neighbors P3HTs is two.

DOI: 10.1103/PhysRevLett.121.026101

Robust relationships between structure and function are generally lacking in organic photovoltaic thin film bulk heterojunction (BHJ) active layers. This is partially due to a lack of measurement tools capable of unveiling structural details at fine enough length scales to be relatable to intermolecular energy transfer. Common analytical methods such as optical spectroscopy, microscopy (AFM, TEM), and scattering techniques do not have sufficient spatial resolution. Solid state NMR can measure internuclear distances in the absence of long-range order by detecting heteronuclear dipolar couplings, making it attractive for characterizing mesoscale order in disordered soft matter materials. One robust technique is rotational echo double resonance (REDOR). In REDOR, the local dipolar field created by a nearby nucleus dephases the detected nucleus with inverting  $\pi$  pulses. Since dipolar couplings are proportional to the inverse cube of the internuclear distance, REDOR can be selective to donor-to-acceptor contacts at the interface. We demonstrate the first such measurement in a bulk heterojunction and show that the data can constrain molecular packing models in the mixed phase and measure the fraction of donor-acceptor nearest neighbors.

In this Letter, we present  $^{13}\text{C}$ -detect,  $^2\text{H}$ -dephase REDOR results that were used to measure dipolar couplings between fullerene  $^{13}\text{C}$  nuclei in  $^{13}\text{C}$ -enriched phenyl- $\text{C}_{60}$ -butyric acid

methyl ester (PCBM) and  $^2\text{H}$  nuclei on the  $^2\text{H}$ -enriched beta-hydrogen positions on the poly(3-hexyl thiophene) (P3HT) main chain. Synthesis details are given in the Supplemental Material [1]. We propose a simple cuboid lattice model of PCBM and P3HT that is used to fit the REDOR data and discuss, based on these fits, the local domain compositions. Despite several interrelated variables and the lack of a unique model structure, we unambiguously conclude that even in films with a high level of mixing as shown from TEM, differential scanning calorimetry (DSC), and  $^1\text{H}$  spin diffusion NMR: (1) the average PCBM molecule is next to two P3HT chains, (2) neat PCBM clusters form on  $\leq 3$  nm length scales but not on length scales  $\geq 6$  nm, and (3) the small angle neutron scattering correlation peak at  $q = 0.03 \text{ \AA}^{-1}$  is due to spatial correlations in the mixed phase.

Interfacial structures are probed via NMR by utilizing an isotopic labeling scheme. Labeled P3HT was synthesized with deuterium on the thiophene rings. PCBM was synthesized by functionalizing  $18\%$   $^{13}\text{C}$ -enriched  $\text{C}_{60}$ . The enrichment level of  $\text{C}_{60}$  was intentionally set to increase the sensitivity while minimizing the fraction of directly bonded  $^{13}\text{C} - ^{13}\text{C}$  pairs that prohibit meaningful REDOR experiments due to the large ( $\approx 120$  Hz) homonuclear  $J$  couplings. The BHJ blend film for this study has low polymer crystallinity and is well mixed (see below). Distributions of

$^{13}\text{C}$  –  $^2\text{H}$  dipolar couplings are used to determine the likely candidate structures in the mixed phase by comparing the REDOR data to simulated curves using atomic positions in a simple cuboid lattice model.

We prepared BHJ films from the isotopically labeled P3HT and PCBM using a doctor blading technique [16,17]. Our casting conditions were chosen to mimic typical organic solar cell casting with a target film thickness of  $\approx 80$  nm and solid mass fraction of PCBM of 0.5. Single films were fabricated over large areas ( $15 \times 15$  cm<sup>2</sup>) to maximize the amount of the sample for the NMR measurement (12 mg), then delaminated upon submerging into water. We purposefully used a relatively volatile solvent (chlorobenzene) with a short drying time ( $< 10$  s) and did not thermally anneal the films, with the goal of maximizing the amount of amorphous mixed phase to obtain more signal from this phase in our NMR measurements. In typical organic solar cell production, such films would be thermally annealed to increase P3HT crystallinity and reduce the amount of the amorphous mixed phase, which typically improves the power conversion efficiency.

Our BHJ films were first studied by conventional techniques to determine the extent of crystallinity and provide us with an estimate of the amount and composition of the mixed phase. A low crystallinity and predominant mixed phase are supported by energy filtered TEM (Fig. S1 in the Supplemental Material [1]). No P3HT fibrils or other dominant domains are observed. The slight fluctuations in imaging contrast are difficult to ascribe to domain composition because of the competing effects of variations in electron density and thickness. From DSC (Fig. S2 in the Supplemental Material [1]), we measure the absolute P3HT crystallinity to be  $0.27 \pm 0.03$  using an approach we describe elsewhere [18] that employs the Flory-Huggins parameter ( $\chi = 0.86 \pm 0.09$ ) [5], infinite chain melt temperature ( $T_m^0 = 545 \pm 6$  K), and infinite chain melt enthalpy ( $\Delta H_u = 49 \pm 2$  J/g). From the melting temperature suppression, we estimate a chain length ( $c$  axis) crystal thickness of 17 nm (or 33 repeat units) [18,19]. Grazing incidence x-ray diffraction shows P3HT form I [20] crystals (Fig. S3 in the Supplemental Material [1]). The widths of the (100) and (020) reflections correlate to coherent length scales of  $\approx 10$  nm in the  $a$ -axis (side chain) direction and  $\approx 5$  nm in the  $b$ -axis ( $\pi$ -stacking) direction, respectively. With a P3HT mass fraction of  $0.50 \pm 0.02$ , the DSC-determined crystallinity constrains the global mixed phase P3HT mass fraction to be 0.42. Assuming densities of 1.1 and 1.5 g/cm<sup>3</sup> for P3HT and PCBM, respectively, the P3HT volume fraction is 0.50, which agrees well with the scattering length density observed via x-ray reflectivity (Fig. S4 in the Supplemental Material [1]).

We measured the miscibility in the BHJ using  $^1\text{H}$  spin diffusion NMR methods previously demonstrated [21]. The  $^1\text{H}$  spin diffusion NMR (Fig. S5 in the Supplemental Material [1]) reveals a high level of mixing, as shown in

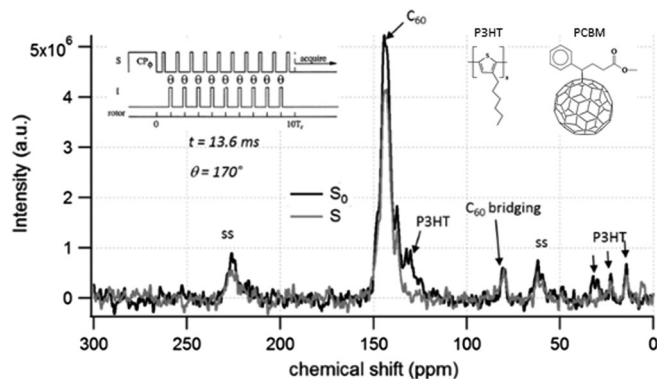


FIG. 1.  $^{13}\text{C}$  cross polarization magic angle spinning spectra both without (black) and with (gray)  $^2\text{H}$  REDOR dephasing pulses. The REDOR pulse sequence is given above. The dephasing time was 13.6 ms.

similarly prepared films [21]. Using composition constraints from the spin diffusion NMR [22], we determine (1) an upper bound of P3HT crystallinity of  $\approx 0.4$ , (2) that approximately 80% of the film is mixed on  $\leq 6$  nm size scales, and (3) the mixed phase contains more than 0.37 mass fraction of P3HT, in general good agreement with the DSC. Domain sizes from spin diffusion are not precise at  $< 5$  nm length scales in the P3HT/PCBM BHJ blends.

REDOR is a powerful high-resolution solid state NMR probe of heteronuclear dipolar couplings. Internuclear distances between heteroatoms can be measured via the  $r^{-3}$  dependence of dipolar fields making REDOR an attractive measurement for local structure, even in systems with no long-range order. Since its inception, REDOR has been utilized for structural characterization of amyloid fibrils [23,24], influenza protein binding sites [25], metal oxide glasses [26,27], peptides [28], metal organic frameworks [29], and many other solids. We collected REDOR spectra for dephasing times ranging from 2 to 21 ms. Shown in Fig. 1 are REDOR spectra taken with 13.6 ms of dephasing time both with (gray curve) and without (black curve) the  $^2\text{H}$  dephasing pulses, which are denoted  $S_0$  and  $S$ . REDOR dephasing defined as  $\Delta S(t)/S_0(t) = [S_0(t) - S(t)]/S_0(t)$  will be observed for  $^{13}\text{C}$  nuclei that are proximal to dephasing  $^2\text{H}$  nuclei. There are multiple resonances in the spectra, but we focus on the primary  $\text{C}_{60}$   $^{13}\text{C}$  resonance at 144 ppm. There is observable REDOR dephasing ( $\Delta S/S_0 > 0$ ) of the  $\text{C}_{60}$  peak, which is due to the fullerene  $^{13}\text{C}$  nuclei adjacent to the deuterons on P3HT chains in the mixed phase. (Large error bars for the weaker resonance at 80 ppm prevented meaningful analysis.) The experimentally observed  $\Delta S/S_0$  is not a simple binary interaction, and one must consider many potential participant nuclei precluding simple extraction of an internuclear distance; a molecular packing model is required.

*Modeling REDOR dephasing of P3HT/PCBM from a simple cuboid lattice model.*—PCBM is in the mixed phase, so the number of neighboring P3HT chains are not known.

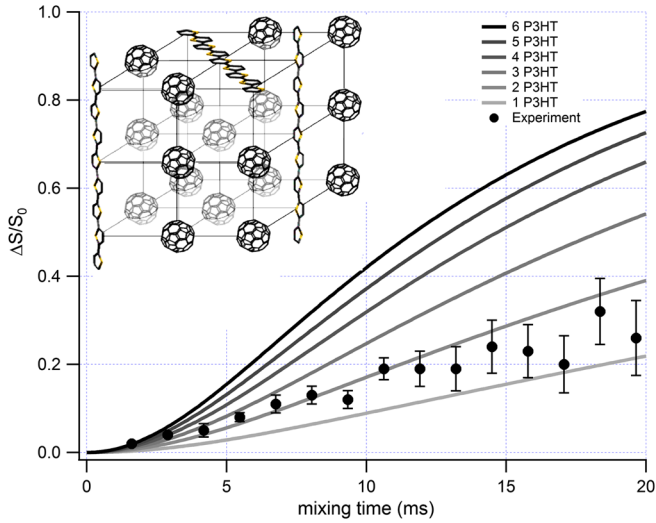


FIG. 2. Experimental (dots) and simulated (lines) REDOR curves. The gray and black lines get darker with increasing  $(3\text{HT})_9$  content. The lines correspond to  $(3\text{HT})_9$  on the face(s) of the cuboid and no  $(3\text{HT})_9$  on the corners. Dotted lines correspond to cuboids with  $(3\text{HT})_9$  molecules on the cuboid and  $(3\text{HT})_9$  molecules on all four corners.

To systematically address the possible structures surrounding a given fullerene, we modeled the REDOR data using atomic positions from PCBM and P3HT on a simple cuboid lattice, which places PCBM in the center of a cuboid with six nearest neighbors at the face of the cube (distance  $a/2$ ), 12 next nearest neighbors at the edges (distance  $\sqrt{2}a/2$ ), and eight next, next nearest neighbors at the corners (distance  $\sqrt{3}a/2$ ). The  $^{13}\text{C}$  nuclei are randomly distributed in  $\text{C}_{60}$ , so we include all fullerene carbons. In this model, each lattice site is either  $\text{C}_{60}$  or a terthiophene molecule  $(3\text{HT})_3$ . An example is given in Fig. 2 (inset). The  $(3\text{HT})_3$  units are linked together along the chain axis in units of three to form  $(3\text{HT})_9$ , so  $(3\text{HT})_3$  always occupies three adjacent sites. Each thiophene is  $3.9 \text{ \AA}$  long along the main chain, so polymer connectivity necessitates the cell dimension that includes thiophene set to  $11.7 \text{ \AA} (= 3 \times 3.9 \text{ \AA})$ . Deuterons on segments farther away than the  $(3\text{HT})_9$  contribute  $<0.5\%$  to the REDOR dephasing within the 20 ms timescale of the experiment (Fig. S6 in the Supplemental Material [1]). For cuboids with greater than four  $(3\text{HT})_9$  units, additional  $(3\text{HT})_9$  units are placed along the diagonal of a given face since the edge sites are fully occupied. The  $(3\text{HT})_3$  hydrogen atom positions were taken from the interior three thiophene monomers from the quinquethiophene [30] crystal structure, and the fullerene carbons were taken from the PCBM [31] crystal structure. The P3HT persistence length in good solvent is  $3.0 \text{ nm}$  at room temperature [32], and we are assuming  $(3\text{HT})_9$  is a  $3.5 \text{ nm}$  long rigid rod, which is perhaps unrealistic. However, even if there is chain curvature farther away from the  $\text{C}_{60}$ , the more distant deuterons contribute much

less to  $\Delta S/S_0$  than those of closest approach (Fig. S6 of the Supplemental Material [1]) and will not affect our conclusions significantly.

Explicit density matrix calculations of large ( $>100$ ) spin systems such as these are computationally unreasonable, particularly when considering the numerous possible configurations. For simplicity, we leveraged the pairwise additivity of the heterospin couplings to determine an “effective” field. While one could, in principle, sum the individual dipolar oscillations and integrate over all orientations, we utilized the fact that (1)  $\Delta S/S_0$  for a given coupling will go as  $[1 - e^{-(D_{ij}t)^2}]$  [33], and (2)  $\Delta S/S_0$  from multiple spins goes as the heteronuclear second moment [34], and instead, we use

$$\frac{\Delta S}{S_0}(t_m)_{\text{comp}} = \sum_{j=1}^{60} \left( 1 - \prod_{i=1}^n \frac{1 - \left(\frac{\Delta S}{S_0}\right)_{i,j}}{0.6} \right) \approx \frac{1}{60} \sum_{j=1}^{60} \left\{ 1 - \prod_{i=1}^n \exp \left[ \frac{-(kD_{ij}t_m)^2}{0.6} \right] \right\}, \quad (1)$$

where  $i$  and  $j$  are the  $^2\text{H}$  and  $^{13}\text{C}$  spins, respectively,  $D_{ij}$  is the dipolar coupling constant between spins  $i$  and  $j$ ,  $t_m$  is the mixing time,  $(\Delta S/S_0)_{i,j}$  corresponds to the REDOR intensity of spins  $i$  and  $j$ , and  $k(=1.7)$  is an empirically determined proportionality constant based on density matrix simulations and experiments on L-alanine- $3\text{-}^{13}\text{C}$ ,  $^2\text{H}$ - (Figs. S7–S9 in the Supplemental Material [1]).

Simulated REDOR curves were calculated using Eq. (1) for different fractions of terthiophene sites, including possible nondegenerate coordination arrangements (i.e., adjacent vs opposite) for different P3HT-to-PCBM orientations and two P3HT-to-PCBM distances  $a/2 = 8$  or  $8.6 \text{ \AA}$ , corresponding to low- and high-density packing  $1.3$  and  $1.6 \text{ g/cm}^3$ , respectively. For a fixed P3HT fraction, the effect of arrangement type (i.e., three adjacent vs two adjacent, one opposite terthiophene) on  $\Delta S/S_0$  is small compared to the density and orientation effects (Figs. S10 and S11 in the Supplemental Material [1]). The curves were averaged over different orientations and densities, and the results are given in Fig. 2 for different numbers of  $(3\text{HT})_3$  on the faces of the cuboid ranging from one to six. Adding the  $(3\text{HT})_3$  on the corner sites contributes negligibly to the dephasing (Fig. S12 in the Supplemental Material [1]), which demonstrates the REDOR dephasing rate is directly proportional to the number of  $(3\text{HT})_3$  on the faces of the cuboid, and, therefore, REDOR is a sensitive probe of nearest neighbor contacts.

As shown in Fig. 2, the experimental data lie between the curves predicted for cuboids with one and two P3HTs. If our model’s stoichiometry was identical to the sample’s global stoichiometry ( $0.42\text{P3HT} \times 0.58\text{PCBM}$ ), then the data would be in between the curves predicted for three- and four-face  $(3\text{HT})_3$  molecules. The lack of agreement

with experiment suggests that our model, which assumes a mixed phase that is uniformly mixed at  $\approx 2$  nm length scales, is fundamentally inconsistent with the mixed phase of the BHJ. There must be domains on the size scale of our model ( $\approx 2$  nm) that deviate from the global composition that are enriched in either P3HT or PCBM. In other words, the BHJ mixed phase cannot be built up from compositionally *identical* units as small as our simple cuboid model but can be built up from compositionally *varying* cuboid structures. From our  $^1\text{H}$  spin diffusion data, we know that the mixed phase is compositionally uniform on  $\approx 6$  nm length scales, so groupings of 20–40 cuboids ( $>6$  nm on a side) must approach the global composition.

In principle, one could fully quantify the distribution of cuboids of different compositions by fitting the REDOR data to a linear combination of the curves (as shown in Fig. 2) along with a curve corresponding to PCBM with no surrounding  $(3\text{HT})_3$  ( $\Delta S/S_0 = 0$  for all times) and by using the global mass fraction of P3HT in the mixed phase (0.42) as a constraint. Unfortunately, there is not a unique fit since the local compositions, densities, and relative orientations of the molecules are not known, and their effects are too significant to disregard. Alternatively, we simply estimated the fraction of interfacial contacts for the possible configurations in our model. We assumed a trimodal distribution (neat P3HT, neat PCBM, and mixed composition) and fit the data to linear combinations of curves corresponding to neat PCBM ( $\Delta S/S_0 = 0$  for all times) and the various simulated curves (Fig. 2, and Fig. S11 in the Supplemental Material [1]). The fraction of neat P3HT was calculated via mass balance. The volume fraction of P3HT  $\Phi_{\text{P3HT}} = 0.50$  was estimated assuming literature values of the density for P3HT and PCBM [35] and was used to constrain the fit using

$$\Phi_{\text{P3HT}} = \sum_{i=0}^{n=8} \phi_i f_i, \quad (2)$$

where  $\phi_i$  is the P3HT volume fraction of a cuboid that includes  $i$   $(3\text{HT})_9$  molecules,  $f_i$  is the fraction of those cuboids, and  $\sum_{i=0}^{n=8} f_i = 1$ . The fits were weighted based on the error bars, and the resultant volume fractions were calculated (Table S1 in the Supplemental Material [1]) for different values of the fraction of neat PCBM ( $f_0$ ), neat P3HT ( $f_8$ ), and mixed composition ( $f_1 - f_6$ ) cuboids for different  $(3\text{HT})_3$  orientations and densities. From all the different orientations and densities (Fig. 2, and Fig. S11 in the Supplemental Material [1]), the average fraction of P3HT nearest neighbors for the average PCBM molecule ( $n f_n / 6 f_n + 6 f_0$ ) is 0.33 with a spread of  $\pm 0.06$ . This corresponds to approximately two P3HT molecules next to PCBM on average, a factor of 2 smaller than expected from the mixed phase composition, suggesting the presence of neat P3HT and PCBM clusters in the mixed phase ( $\geq 3$  nm).

A powerful method for probing spatial composition heterogeneity is small angle neutron scattering (SANS),

and there have been multiple P3HT/PCBM studies. Yin and Dadmun [8] attributed the SANS correlation peak to P3HT crystals dispersed homogeneously in a mixture of amorphous PCBM and P3HT. Mackay and co-workers [36] reported a real-space model with  $\approx 5$  nm domains that fit the SANS curve with no P3HT crystals explicitly added. We examined our sample with SANS (Fig. 3), and the scattering curve was fit to an empirical correlation length model given by

$$I(q) = \frac{A}{q^n} + \frac{C}{1 + (q\xi)^m} + B, \quad (3)$$

where  $A$  and  $C$  are scaling coefficients,  $B$  is the background incoherent scattering,  $n$  and  $m$  are the Porod and Lorentzian exponents, respectively, and  $\xi$  is the correlation length. Fits to this curve yielded  $n = 2.9$ ,  $m = 3.7$ , and a correlation length of 3.3 nm, which we posit is due to spatial correlations in the mixed phase. There is significant scattering intensity at  $q < 0.01 \text{ \AA}^{-1}$ , which corresponds to length scales of the order of the crystal-crystal separation distance ( $>80$  nm) and the film thickness ( $\approx 80$  nm). This low- $q$  feature was subtracted from the raw data using the first term in Eq. (3), and we calculated the total scattering invariant (TSI) of the resultant curve to be  $0.0052 \text{ cm}^{-1} \text{ \AA}^{-1}$ . This value is close to what one would predict if the scattering for  $q > 0.01 \text{ \AA}^{-1}$  is due to contrast between P3HT and PCBM molecules over short length scales in the mixed phase using

$$\text{TSI} = 2\pi\phi(1 - \phi)(\Delta\rho)^2, \quad (4)$$

where  $\phi$  is the volume fraction of one of the phases, and  $\Delta\rho$  is the difference in scattering length densities of P3HT and PCBM.

We calculated the spatial correlation function in order to predict the probability of finding a PCBM at a face site in our cuboid model. The scattering curve was converted to evenly spaced data points in the  $q$  dimension using interpolation, then Fourier transformed numerically to obtain the spatial correlation function [Fig. 3(b)]. At displacements of  $\Delta r = (0.8-1)$  nm, we observe a value of  $I(r) \times I(r + \Delta r) \approx 0.7$ , from which we calculate the probability of PCBM being at a face site to be 0.85. The probability density distribution of cuboids follows a binomial distribution [Fig. 3(c)], and the greatest populations are with PCBM either fully surrounded by PCBM molecules or with low P3HT coordination. Structures that include PCBM coordinated with higher numbers of P3HT molecules (more than three) only occur in low densities ( $<3\%$ ), which is consistent with our REDOR findings. This suggests that the SANS intensity for  $q > 0.01 \text{ \AA}^{-1}$  is due to scattering within the mixed phase.

Why do we observe 2–3 nm neat domains in an otherwise well-mixed phase? First, even in miscible liquids, neat clusters can be predicted from the Kirkwood-Buff

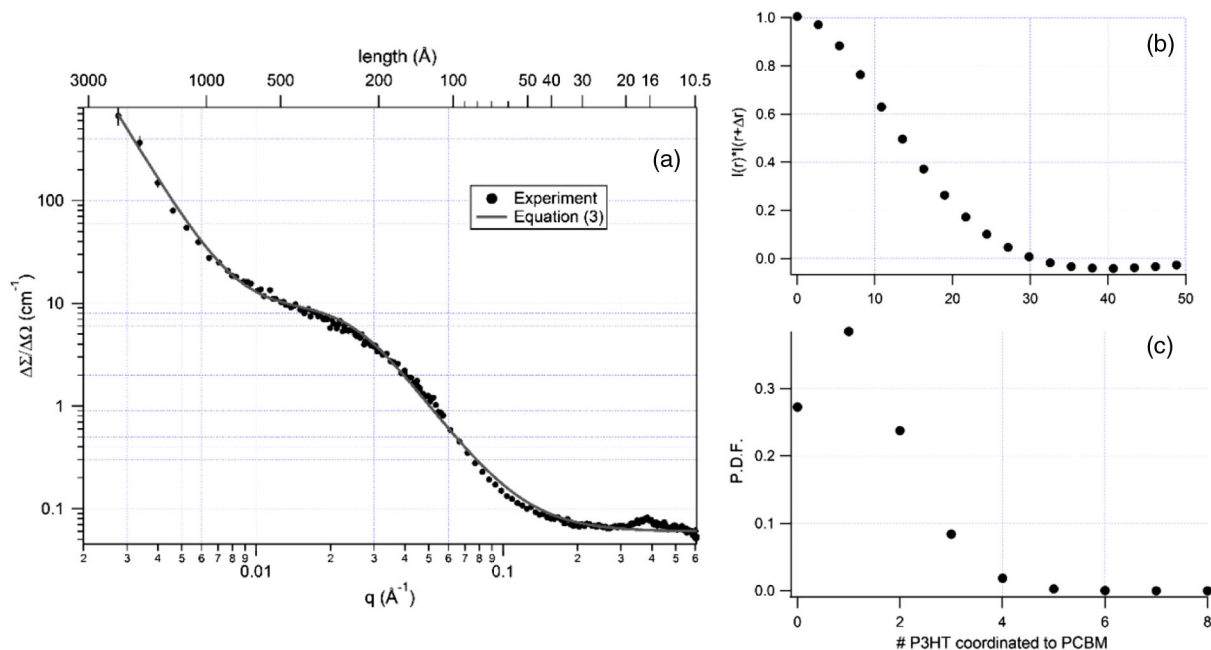


FIG. 3. (a) Small angle neutron scattering curve of P3HT/PCBM (dots) and model fits. (b) The spatial correlation function for a value of  $\zeta = 3.3$  nm. (c) The probability distribution for finding  $(3HT)_3$  on the face of the simple cubic lattice assuming a 0.15 probability and a binomial distribution.

theory of solutions depending on the chemical potentials, molecular volumes, and activity coefficients [37,38]. A Kirkwood-Buff analysis showed that differences in chain rigidity [39] and molecular shape [40] can cause longer-range composition heterogeneity. Furthermore, we should recall that  $\chi > 0.5$  for P3HT/PCBM, which ranks PCBM as a poor solvent for P3HT. Recent theoretical work [41,42] suggests that for  $\chi > 0.5$ , dilute polymer chains in solution form compact globules. For P3HT/PCBM ( $\chi = 0.86$ ), dilute P3HT in PCBM solution would be in a “swollen globule” state in which there would be a greater than fivefold increase in the local polymer volume fraction above that from  $\chi = 0.5$  (Fig. 1 in Ref. [2]).

Using a simple cuboid model, we demonstrate that  $^{13}\text{C}$   $\{^2\text{H}\}$  REDOR can quantify the near neighbor contacts between PCBM and P3HT in the amorphous interphase in bulk heterojunction thin film blends. Surprisingly, given the balanced volume fractions, we find that for the average PCBM molecule, the fraction of P3HT-to-PCBM nearest neighbor contacts is small (0.3) and that neat P3HT and PCBM clusters exist on  $\geq 3$  nm size scales. Quantitative comparison of the NMR results and SANS demonstrates that the scattering at  $q > 0.01 \text{ \AA}^{-1}$  likely arises from these small clusters. Future work will focus on annealed blends that possess a larger fraction of crystalline pure phase so that these interphase structures can be correlated to function and device processing, noting that effects of isotope labeling on device performance have been reported [43]. We expect to extend this technique to other soft matter application areas such as structural materials and biological

materials, where the quantitative characterization of the interfacial structure is important.

D.L. VanderHart, J. Schaefer, and C.L. Soles are acknowledged for their thoughtful comments and edits of this manuscript. Portions of this work benefited from and provided support to the National Institute of Standards and Technology (NIST) nSoft consortium, including use of the 10 m small angle neutron scattering instrument at the NIST Center for Neutron Research. This work was carried out by the NIST, an agency of the U.S. government, and by statute is not subject to copyright in the United States. Certain commercial equipment, instruments, materials, services, or companies are identified in this paper in order to specify adequately the experimental procedure. This in no way implies endorsement or recommendation by NIST.

\*ryann@nist.gov

- [1] See the Supplemental Material at <http://link.aps.org/supplemental/10.1103/PhysRevLett.121.026101> for a description of the synthesis, experimental details, transmission electron microscopy, differential scanning calorimetry, x-ray diffraction, x-ray reflectivity, NMR simulations, and slow MAS  $^{13}\text{C}$  CPMAS spectrum of P3HT/PCBM, which includes Refs. [2–15].
- [2] Z. Fei, P. Boufflet, S. Wood, J. Wade, J. Moriarty, E. Gann, E. L. Ratcliff, C. R. McNeill, H. Siringhaus, J.-S. Kim, and M. Heeney, Influence of backbone fluorination in regioregular poly(3-alkyl-4-fluoro)thiophenes, *J. Am. Chem. Soc.* **137**, 6866 (2015).

- [3] C. R. Morcombe and K. W. Zilm, Chemical shift referencing in MAS solid state NMR, *J. Magn. Reson.* **162**, 479 (2003).
- [4] S. R. Kline, Reduction and analysis of SANS and USANS data using IGOR Pro, *J. Appl. Crystal.* **39**, 895 (2006).
- [5] D. R. Kozub, K. Vakhshouri, L. M. Orme, C. Wang, A. Hexemer, and E. D. Gomez, Polymer crystallization of partially miscible polythiophene/fullerene mixtures controls morphology, *Macromolecules* **44**, 5722 (2011).
- [6] B. Crist and F. M. Mirabella, Crystal thickness distributions from melting homopolymers or random copolymers, *J. Polym. Sci. B* **37**, 3131 (1999).
- [7] C. Snyder, D. M. DeLongchamp, R. C. Nieuwendaal, and A. A. Herzing, in *Semiconducting Polymers: Controlled Synthesis and Microstructure*, edited by C. Luscombe (Royal Society of Chemistry, Cambridge, 2016), Ch. 7, p. 219.
- [8] W. Yin and M. Dadmun, A new model for the morphology of P3HT/PCBM organic photovoltaics from small-angle neutron scattering: Rivers and streams, *ACS Nano* **5**, 4756 (2011).
- [9] P. J. Flory, Thermodynamics of crystallization in high polymers. IV. A theory of crystalline states and fusion in polymers, copolymers, and their mixtures with diluents, *J. Chem. Phys.* **17**, 223 (1949).
- [10] L. Mandelkern and P. J. Flory, Melting and glassy state transitions in cellulose esters and their mixtures with diluents, *J. Am. Chem. Soc.* **73**, 3206 (1951).
- [11] P. J. Flory, *Principles of Polymer Chemistry* (Cornell University Press, Ithaca, 1953).
- [12] J. Ilavsky, Nika: software for two-dimensional data reduction, *J. Appl. Crystallogr.* **45**, 324 (2012).
- [13] H. Sirringhaus, P. J. Brown, R. H. Friend, M. M. Nielsen, K. Bechgaard, B. M. W. Langeveld-Voss, A. J. H. Spiering, R. A. J. Janssen, E. W. Meijer, P. Herwig, and D. M. de Leeuw, Two-dimensional charge transport in self-organized, high-mobility conjugated polymers, *Nature (London)* **401**, 685 (1999).
- [14] R. C. Nieuwendaal, C. R. Snyder, R. J. Kline, E. K. Lin, D. L. VanderHart, and D. M. DeLongchamp, Measuring the extent of phase separation in poly-3-hexylthiophene/phenyl-C<sub>61</sub>-butyric acid methyl ester photovoltaic blends with <sup>1</sup>H spin diffusion NMR spectroscopy, *Chem. Mater.* **22**, 2930 (2010).
- [15] C. S. Yannoni, R. D. Johnson, G. Meijer, D. S. Bethune, and J. R. Salem, Carbon-13 NMR study of the C<sub>60</sub> cluster in the solid state: molecular motion and carbon chemical shift anisotropy, *J. Phys. Chem.* **95**, 9 (1991).
- [16] C. M. Stafford, K. Roskov, T. H. Epps, and M. J. Fasolka, Generating thickness gradients of thin polymer films via flow coating, *Rev. Sci. Instrum.* **77**, 023908 (2006).
- [17] N. Shin, L. J. Richter, A. A. Herzing, R. J. Kline, and D. M. DeLongchamp, Effect of processing additives on the solidification of blade-coated polymer/fullerene blend films via in-situ structure measurements, *Adv. Energy Mater.* **3**, 938 (2013).
- [18] C. R. Snyder, R. C. Nieuwendaal, D. M. DeLongchamp, C. K. Luscombe, P. Sista, and S. D. Boyd, Quantifying crystallinity in high molar mass poly(3-hexylthiophene), *Macromolecules* **47**, 3942 (2014).
- [19] M. G. Broadhurst, Extrapolation of the orthorhombic n-paraffin melting properties to very long chain lengths, *J. Chem. Phys.* **36**, 2578 (1962).
- [20] T. J. Prosa, M. J. Winokur, J. Moulton, P. Smith, and A. J. Heeger, X-ray structural studies of poly(3-alkylthiophenes): An example of an inverse comb, *Macromolecules* **25**, 4364 (1992).
- [21] R. C. Nieuwendaal, H. W. Ro, D. S. Germack, R. J. Kline, M. F. Toney, C. K. Chan, A. Agrawal, D. Gundlach, D. L. VanderHart, and D. M. DeLongchamp, Measuring domain sizes and compositional heterogeneities in P3HT-PCBM bulk heterojunction thin films with <sup>1</sup>H spin diffusion NMR spectroscopy, *Adv. Funct. Mater.* **22**, 1255 (2012).
- [22] R. C. Nieuwendaal, C. R. Snyder, R. J. Kline, E. K. Lin, D. L. VanderHart, and D. M. DeLongchamp, Measuring the extent of phase separation in poly-3-hexylthiophene/phenyl-C<sub>61</sub>-butyric acid methyl ester photovoltaic blends with <sup>1</sup>H Spin diffusion NMR spectroscopy, *Chem. Mater.* **22**, 2930 (2010).
- [23] A. T. Petkova, W. M. Yau, and R. Tycko, Experimental constraints on quaternary structure in Alzheimer's  $\beta$ -amyloid fibrils, *Biochemistry* **45**, 498 (2006).
- [24] J. J. Balbach, Y. Ishii, N. Antzutkin, R. D. Leapman, N. W. Rizzo, F. Dyda, J. Reed, and R. Tycko, Amyloid fibril formation by A $\beta$ <sub>16-22</sub>, a seven-residue fragment of the Alzheimer's  $\beta$ -amyloid peptide, and structural characterization by solid state NMR, *Biochemistry* **39**, 13748 (2000).
- [25] S. D. Cady, K. Schmidt-Rohr, J. Wang, C. S. Soto, W. F. DeGrado, and M. Hong, Structure of the amantadine binding site of influenza M2 proton channels in lipid bilayers, *Nature (London)* **463**, 689 (2010).
- [26] H. Eckert, Structural characterization of noncrystalline solids and glasses using solid state NMR, *Prog. Nucl. Magn. Reson. Spectrosc.* **24**, 159 (1992).
- [27] J. C. C. Chan, M. Bertmer, and H. Eckert, Site connectivities in amorphous materials studied by double-resonance NMR of quadrupolar nuclei: High-resolution <sup>11</sup>B  $\leftrightarrow$  <sup>27</sup>Al spectroscopy of aluminoborate glasses, *J. Am. Chem. Soc.* **121**, 5238 (1999).
- [28] C. M. Rienstra, L. Tucker-Kellogg, C. P. Jaroniec, M. Hohwy, B. Reif, M. T. McMahon, B. Tidor, T. Lozano-Perez, and R. G. Griffin, De novo determination of peptide structure with solid-state magic-angle spinning NMR spectroscopy, *Proc. Natl. Acad. Sci. U.S.A.* **99**, 10260 (2002).
- [29] X. Q. Kong, H. X. Deng, F. Y. Yan, J. Kim, J. A. Swisher, B. Smit, O. M. Yaghi, and J. A. Reimer, Mapping of functional groups in metal-organic frameworks, *Science* **341**, 882 (2013).
- [30] W. Porzio, S. Destri, M. Mascherpa, and S. Bruckner, Structural aspects of oligothiophenyl series from X-ray powder diffraction data, *Acta Polym.* **44**, 266 (1993).
- [31] M. T. Rispens, A. Meetsma, R. Rittberger, C. J. Brabec, N. S. Sariciftci, and J. C. Hummelen, Influence of the solvent on the crystal structure of PCBM and the efficiency of MDMO-PPV:PCBM 'plastic' solar cells, *Chem. Commun. (Cambridge)* 2116 (2003).
- [32] B. McCulloch, V. Ho, M. Hoarfrost, C. Stanley, C. Do, W. T. Heller, and R. A. Segalman, Polymer chain shape of

- poly(3-alkylthiophenes) in solution using small-angle neutron scattering, *Macromolecules* **46**, 1899 (2013).
- [33] E. Hughes, T. Gullion, A. Goldbourt, S. Vega, and A. J. Vega, Internuclear distance determination of  $S = 1$ ,  $I = 1/2$  spin pairs using REAPDOR NMR, *J. Magn. Reson.* **156**, 230 (2002).
- [34] M. Bertmer and H. Eckert, Dephasing of spin echoes by multiple heteronuclear dipolar interactions in rotational echo double resonance NMR experiments, *Solid State Nucl. Magn. Reson.* **15**, 139 (1999).
- [35] H. W. Ro, B. Akgun, B. T. O'Connor, M. Hammond, R. J. Kline, C. R. Snyder, S. K. Satija, A. L. Ayzner, M. F. Toney, C. L. Soles, and D. M. DeLongchamp, Poly(3-hexylthiophene) and [6,6]-phenyl-C61-butyric acid methyl ester mixing in organic solar cells, *Macromolecules* **45**, 6587 (2012).
- [36] D. P. Olds, P. M. Duxbury, J. W. Kiel, and M. E. Mackay, Percolating bulk heterostructures from neutron reflectometry and small-angle scattering data, *Phys. Rev. E* **86**, 061803 (2012).
- [37] J. G. Kirkwood and F. P. Buff, The statistical mechanical theory of solutions. I, *J. Chem. Phys.* **19**, 774 (1951).
- [38] I. Shulgin and E. Ruckenstein, The Kirkwood–Buff theory of solutions and the local composition of liquid mixtures, *J. Phys. Chem. B* **110**, 12707 (2006).
- [39] J. Dudowicz, K. F. Freed, and J. F. Douglas, Concentration fluctuations in miscible polymer blends: Influence of temperature and chain rigidity, *J. Chem. Phys.* **140**, 194901 (2014).
- [40] J. Dudowicz, J. F. Freed, and J. F. Douglas, The osmotic virial formulation of the free energy of polymer mixing, *J. Chem. Phys.* **116**, 9983 (2002).
- [41] R. Wang and Z. G. Wang, Theory of polymers in poor solvent: Phase equilibrium and nucleation behavior, *Macromolecules* **45**, 6266 (2012).
- [42] R. Wang and Z. G. Wang, Theory of polymer chains in poor solvent: Single-chain structure, solution thermodynamics, and  $\Theta$  point, *Macromolecules* **47**, 4094 (2014).
- [43] M. Shao, J. Keum, J. Chen, Y. He, W. Chen, J. F. Browning, J. Jakowski, B. G. Sumpter, I. N. Ivanov, Y. Z. Ma, C. Rouleau, S. C. Smith, D. B. Geohegan, K. Hong, and K. Xiao, The isotopic effects of deuteration on optoelectronic properties of conducting polymers, *Nat. Commun.* **5**, 3810 (2014).